

Observational Possibility of the “Snow Line” on the Surface of Circumstellar Disks with the Scattered Light

Akio K. INOUE

College of General Education, Osaka Sangyo University, 3-1-1, Nakagaito, Daito 574-8530

akinoue@las.osaka-sandai.ac.jp

Mitsuhiko HONDA

Department of Information Science, Kanagawa University, 2946 Tsuchiya, Hiratsuka, Kanagawa 257-0031

hondamt@kanagawa-u.ac.jp

Taishi NAKAMOTO

and

Akinori OKA

Department of Earth and Planetary Sciences, Tokyo Institute of Technology, Ookayama, Meguro, Tokyo 152-8551

nakamoto@geo.titech.ac.jp, akinori@geo.titech.ac.jp

(Received ⟨reception date⟩; accepted ⟨acceptation date⟩)

Abstract

We discuss how we obtain the spatial distribution of ice on the surface of the circumstellar disk around young stars. Ice in the disks plays a very important role in various issues, for instance, on the disk structure, on the planet formation, on the isotopic anomaly in meteorites, and on the origin of the sea on the Earth. Therefore, the spatially resolved observation of the condensation/sublimation front of ice, so-called “snow line” is strongly required. Here, we propose a new method for obtaining the spatially resolved “snow line” on the circumstellar disks by observing $3\ \mu\text{m}$ H_2O ice feature in the scattered light. Based on radiative transfer considerations, we show that the feature is clearly imprinted in the spectrum of the scattered light from both optically thick and thin circumstellar disks. We also show that the scattered light and the H_2O ice feature from protoplanetary disks are detectable and spatially resolvable with the current instruments through a H_2O narrow-band filter around $3\ \mu\text{m}$. Finally, we present a diagnostics of disk dust properties on the $K - \text{H}_2\text{O}$ and $K - L'$ two color diagram.

Key words: circumstellar matter — dust, extinction — planetary systems: protoplanetary disks — radiative transfer

1. Introduction

Ice of water plays many important roles in the protoplanetary disk. First, ice enhances the opacity and affects the disk structure (e.g., Lin, Papaloizou 1980; Pollack et al. 1994; ?). Second, ice enhances the amount of solid material in the disk, which promotes the formation of protoplanets and the core of gaseous planets (e.g., Hayashi, Nakazawa, Nakagawa 1985; Kokubo, Ida 2002). Third, ice evaporation in the inner region of the disk may cause the isotopic anomaly of oxygen found in meteorites (Yurimoto, Kuramoto 2002). Fourth, icy planetesimals or comets may bring water on the Earth (Morbidelli et al. 2000; Raymond, Quinn, Lunine 2004) as well as the innermost part of the disk (Eisner 2007). To discuss these issues in detail, we need the spatial distribution of ice in the disk. Therefore, we should resolve the ice condensation/sublimation front, so-called “snow line”, in the disk.

Ice is found ubiquitously in the molecular cloud and the circumstellar envelope through the prominent $3 \mu\text{m}$ absorption feature (e.g., Gibb et al. 2004). In two edge-on protoplanetary disks, the $3 \mu\text{m}$ ice absorption feature is clearly detected by spectroscopy with the Subaru telescope (Terada et al. 2007). However, we cannot resolve the “snow line” along the line of sight with this method. Observations with the Infrared Space Observatory found 44 and $62 \mu\text{m}$ ice emission feature in some protoplanetary disks (Malfait et al. 1999). However, very low spatial resolution of the far-infrared instrument prevents us from resolving the “snow line”, either.

On the other hand, the scattered light from edge-on protoplanetary disks have already been detected well in the optical to the mid-infrared by very high-resolution imaging with the Hubble Space Telescope and ground-based 8-m telescopes (e.g., Burrows et al. 1996; Koresko 1998; McCabe, Duchêne, Ghez 2003). The scattered light from debris disks have also been detected in the optical to the near-infrared (NIR) (e.g., Smith, Terrile 1984; Golimowski et al. 2006; Kalas, Fitzgerald, Graham 2007). Interestingly, Golimowski et al. (2006) suggest that the existence of icy grains is a possible cause of the observed reddening of the optical scattered light beyond ~ 120 AU in the debris disk of β Pictoris. However, Grigorieva et al. (2007) argue that the photosputtering by ultraviolet photons results in the ice erosion in optically thin disks. To resolve this issue, we should seek a direct evidence of the ice if it exists.

The most important merit of the scattered light observations is the ability to reveal the detailed surface structure of the disks. Indeed, coronagraphic imaging with the Subaru telescope has detected the scattered light from face-on disks in the NIR and revealed the surface structure (Fukagawa et al. 2004; Fukagawa et al. 2006). If an evidence of ice is imprinted in the scattered light, we can resolve the distribution of ice, i.e. “snow line”, with the scattered light. In section 2, we first show that the H_2O ice absorption feature at $3 \mu\text{m}$ is clearly imprinted in the scattered light spectrum, and then, we present a few diagnostics diagrams to check the existence of ice as well as a typical grain size. In section 3, we discuss the observational feasibility of the icy grains with the scattered light. The final section is a summary of this paper.

2. Ice feature in the scattered light

2.1. Observable scattered light

We consider the radiation transfer of only the light scattered by the circumstellar disk. That is, we consider a wavelength where the thermal radiation from the disk is negligible. Let us consider a ray toward an observer as shown in Fig. 1. We set an optical depth coordinate t on the ray. For simplicity, we assume that the disk has a clear “surface”. In other words, there is no matter in the outside of the disk. We set the total optical depth of the disk along the ray at the frequency ν as τ_ν^d . Thus, the optical depth coordinate has $t = 0$ and $t = \tau_\nu^d$ at the two “surfaces” of the far and the near sides from the observer, respectively (see Fig. 1). Note that the optical depth $\tau_\nu^d = (\kappa_\nu^a + \kappa_\nu^s)\Sigma$ with the absorption and scattering cross sections per unit gas mass κ_ν^a and κ_ν^s , respectively, and the gas mass column density along the ray Σ . We will assume a typical mass abundance of dust relative to gas based on the elemental abundance of the Sun later. The scattering albedo $\omega_\nu = \kappa_\nu^s / (\kappa_\nu^a + \kappa_\nu^s)$.

The “surface” of the real circumstellar disks can be defined by various ways; the photosphere of the dust emission, the scale height of the material distribution, and the layer at which the optical depth against the stellar radiation becomes unity. For the context of this paper, the last two definitions could be realistic for optically thin and thick disks, respectively. However, we here assume a simpler “surface” in which all the materials are confined. This assumption might be too simple, but we can highlight the relevant physics clearly. In addition, the results from this assumption excellently agree with those from more complicated numerical simulations as shown below.

The observable intensity without the incident radiation along the ray is

$$I_\nu^{\text{obs}} = \int_0^{\tau_\nu^d} S_\nu(t) e^{-(\tau_\nu^d - t)} dt, \quad (1)$$

where $S_\nu(t)$ is the scattering source function along the ray at the optical depth coordinate t shown in Fig. 1. We consider a point P($t[R, z]$) in the disk (see Fig. 1). Assuming the isotropic scattering for simplicity, we have

$$S_\nu(t[R, z]) = \omega_\nu J_\nu^*(R, z) + \omega_\nu J_\nu(t), \quad (2)$$

where J_ν^* is the mean intensity of the stellar radiation;

$$J_\nu^*(R, z) = \frac{1}{4\pi} B_\nu(T_*) \Omega_*(R, z) e^{-\tau_\nu^*(R, z)}, \quad (3)$$

where $B_\nu(T_*)$ is the Planck function with the stellar effective temperature T_* , Ω_* is the solid angle of the stellar photosphere from the point P, and τ_ν^* is the optical depth between the stellar photosphere and the point P. The solid angle is $\Omega_* = \pi f_{\text{vis}} R_*^2 / (R^2 + z^2)$ with the stellar radius R_* and the visible fraction of the stellar photosphere from the point P f_{vis} . If we consider a ray almost face-on and assume a disk geometrically thin, the solid angle Ω_* can be regarded as constant; $\Omega_* = \pi f_{\text{vis}} (R_*/R)^2$. The second term in eq. (2) is due to the multiple scattering in the disk; J is the mean intensity of the scattered radiation at the point P.

In the optically thin disk, we can consider $\tau_\nu^* \approx 0$ and can neglect the multiple scattering; $J \approx 0$. Thus, we have

$$S_\nu(t) \approx S_\nu^* \equiv \omega_\nu B_\nu(T_*) \frac{\Omega_*}{4\pi}, \quad (4)$$

which can be regarded as constant along the ray if Ω_* is approximated to be constant. In this case, we can integrate eq. (1) easily, and we have

$$I_\nu^{\text{obs}} = S_\nu^*(1 - e^{-\tau_\nu^{\text{d}}}) \approx \tau_\nu^{\text{d}} S_\nu^*, \quad (5)$$

where we have applied the condition $\tau_\nu^{\text{d}} \ll 1$ of an optically thin disk.

For the optically thick disk, we can consider $\tau_\nu^* \approx (\tau_\nu^{\text{d}} - t)/\beta$, where β is so-called grazing angle; the angle between the incident radiation and the disk surface (see Fig. 1). Generally, β is as small as about 0.05 radian. Although β increases along the radial distance R from the central star in a flaring disk, we expect $\beta \lesssim 0.1$ radian even at $R \gtrsim 100$ AU (D’Alessio et al. 2006). For a single scattering case, we have

$$S_\nu(t) \approx S_\nu^* e^{-(\tau_\nu^{\text{d}} - t)/\beta}, \quad (6)$$

where S_ν^* is defined in eq. (4). In this case, we can integrate eq. (1) with the assumption of constant β and $1 + 1/\beta \approx 1/\beta$, then,

$$I_\nu^{\text{obs}} \approx \beta S_\nu^*(1 - e^{-\tau_\nu^{\text{d}}/\beta}) \approx \beta S_\nu^*, \quad (7)$$

where we have applied the condition $\tau_\nu^{\text{d}} \gg 1$ of an optically thick disk. However, the multiple scattering could be important for the optically thick disk. According to the ‘‘law of diffuse reflection’’ by semi-infinite plane-parallel medium (Chandrasekhar 1960), this effect is accounted for by the H -function;

$$I_\nu^{\text{obs}}(\mu) \approx \beta S_\nu^* H(\mu, \omega_\nu), \quad (8)$$

where μ is cosine of the reflection angle from the normal of the slab. We have adopted an approximation with $\beta \approx 0$ and $\mu \approx 1$ (i.e. almost face-on).¹

Finally, we have the observable intensity toward the face-on direction as follows:

$$I_\nu^{\text{obs}} \approx \begin{cases} \beta \omega_\nu H(1, \omega_\nu) B_\nu(T_*) \frac{\Omega_*}{4\pi} & \text{(optically thick disk)} \\ \tau_\nu^{\text{d}} \omega_\nu B_\nu(T_*) \frac{\Omega_*}{4\pi} & \text{(optically thin disk)} \end{cases}. \quad (9)$$

Note that $\tau_\nu^{\text{d}} \omega_\nu = \kappa_\nu^{\text{s}} \Sigma = \tau_\nu^{\text{s}}$, where τ_ν^{s} is the scattering optical depth of the disk. Therefore, we can observe the dust feature via the albedo ω_ν or the scattering cross section κ_ν^{s} (or τ_ν^{s}) in the scattered light from circumstellar disks.

¹ The exact form of the ‘‘law of diffuse reflection’’ is (Chandrasekhar 1960, sec. III, eq. 118)

$$I_\nu^{\text{obs}}(\mu) = \omega_\nu \frac{F_\nu}{4} \frac{\mu_0}{\mu + \mu_0} H(\mu, \omega_\nu) H(\mu_0, \omega_\nu),$$

where F_ν is the flux density incident on the plane-parallel slab with the angle from the normal whose cosine is μ_0 . Note that $\mu_0 = \sin \beta \approx \beta \approx 0$, $\omega_\nu F_\nu / 4 = S_\nu^*$ as eq. (4), and $H(0, \omega_\nu) = 1$.

In Fig. 2, we show the scattering albedos and cross sections of silicate and silicate+ice dust as a function of the wavelength in the NIR for some cases of the grain size. The optical properties are taken from Miyake, Nakagawa (1993); astronomical silicate (Draine 1985) and crystalline H₂O ice (Irvine, Pollack 1968; Bertie, Labbé, Whalley 1969; Schaaf, Williams 1973). We calculated the absorption and scattering coefficients of the two species independently by the Mie theory (Bohren, Huffman 1983) with the mass abundances relative to gas of $\zeta_{\text{sil}} = 0.0043$ and $\zeta_{\text{ice}} = 0.0094$ and with the material density of $\delta_{\text{sil}} = 3.3 \text{ g cm}^{-3}$ and $\delta_{\text{ice}} = 0.92 \text{ g cm}^{-3}$ (Miyake, Nakagawa 1993), then, we added them. Even if we calculated the coefficients as ice-coated silicate or silicate-ice mixture, the presence of the H₂O ice features would not be affected qualitatively (Miyake, Nakagawa 1993; Preibisch et al. 1993).

As shown in Fig. 2, we expect in general a steeper spectral slope (i.e. bluer color) as a smaller dust grain size because ω_ν and κ_ν^{s} of smaller grains have a strong wavelength dependence. Since ω_ν and κ_ν^{s} are almost independent of the wavelength, i.e. gray scattering, for $\gtrsim 1 \mu\text{m}$ grains, the spectral slope is expected to be very similar to that of the Rayleigh-Jeans law in the NIR. In the case with H₂O ice, a strong absorption feature of H₂O ice appears in the albedo at $3 \mu\text{m}$ and other features, for example, of $2 \mu\text{m}$ and $4.5 \mu\text{m}$, are also found, but weaker (panel [b]). The $3 \mu\text{m}$ O-H stretching mode also shows the typical resonance feature in the scattering cross section (panel [d]). The strength of the feature seems to decrease as the dust grain size increases although it does not disappear even in the $10 \mu\text{m}$ case.

2.2. Spectrum and color with ice

Fig. 3 shows the expected spectra of the brightness of an annulus with silicate and H₂O ice; the panel (a) is the optically thick case and the panel (b) is the thin case. We have assumed the dust size of $1.0 \mu\text{m}$, the radius of the annulus of 100 AU, and a central A-type star ($T_* = 10,000 \text{ K}$ and $R_* = 2.5 R_\odot$). The gas surface density of the annulus is assumed to be 1.7 g cm^{-2} (e.g., Hayashi, Nakazawa, Nakagawa 1985) and $1.7 \times 10^{-5} \text{ g cm}^{-2}$ for the thick and the thin cases, respectively. The grazing angle $\beta = 0.05$ and the visible fraction of the stellar photosphere $f_{\text{vis}} = 0.5$ are also assumed. The geometry between the observer and the annulus is face-on.

The solid curves in Fig. 3 are calculated by eq. (9). For the optically thick case, we need the H -function. Here we adopt an approximate expression of it by Bridgeman (1988) rather than the original one whose evaluation needs an iterative calculation;

$$H(\mu, \omega_\nu) \approx \frac{1 + 2\mu}{1 + 2\mu\sqrt{1 - \omega_\nu}}. \quad (10)$$

The dotted curves are results from numerical simulations; 1+1D radiative transfer calculation with the variable Eddington factor method developed by Dullemond et al. (2002) but extended by us to treat the isotropic scattering (Inoue, Nakamoto, Oka in preparation). We show the spectra of the single annulus same as the solid curves. In the calculation, we kept $\beta = 0.05$ but iteratively solved the vertical hydrostatic equilibrium in the annulus for the central stellar mass $M_* = 2.5 M_\odot$ to be consistent with

the temperature structure from the radiative equilibrium. As shown in the both panels of Fig. 3, we find excellent agreements between the simple analytic models of eq. (9) and the numerical simulations.

In the NIR around the 3 μm H_2O ice absorption feature, the stellar spectrum can be expressed by the Rayleigh-Jeans law. Thus, as an approximation, the scattered spectra may be given by

$$I_\nu^{\text{obs}} \propto \begin{cases} \omega_\nu \nu^2 & (\text{optically thick disk}) \\ \kappa_\nu^{\text{s}} \nu^2 & (\text{optically thin disk}) \end{cases}, \quad (11)$$

which are shown as the dashed curves in Fig. 3 (see also eq. 13). Indeed, we find that this approximation is good enough to discuss just if the 3 μm H_2O ice feature is observable or not. Hereafter, we use this simple expression as the scattered spectra.

Fig. 4 shows two photometric colors expected as a function of the dust grain size: (a) and (b) for $K - H_2O$, and (c) and (d) for $H_2O - L'$. We have assumed a usual set of the filter transmission functions of K and L' .² This choice of the bands is not definitive. We could choose any two bands shortward and longward of H_2O band.

The H_2O band transmission function is assumed to be a rectangular between 3.02 and 3.16 μm . The magnitude zero points are taken from Cohen et al. (1992) for K and L' . For H_2O , we assume $F_\nu(\text{Vega}) = 357 \text{ Jy}$ at $\lambda = 3.09 \mu\text{m}$ based on Fig. 2 in Cohen et al. (1992). Four disk models, optically thick disk with silicate (open circles), optically thick disk with silicate and ice (filled diamonds), optically thin disk with silicate (open triangles), and optically thin disk with silicate and ice (filled squares), are shown in the panels. The dotted lines indicate the Rayleigh-Jeans law.

The scattered light colors without H_2O ice (open circles and triangles) are bluer than the Rayleigh-Jeans law for a small ($\lesssim 1 \mu\text{m}$) dust size³ and they approach the Rayleigh-Jeans color as the dust size increases. The observational fact that most of the scattered light from the disks are not bluer than the stellar color indicates a large ($\gtrsim 1 \mu\text{m}$) dust size (but AU Mic; Krist et al. 2005).

If the dust includes H_2O ice (filled diamonds and squares), significant differences appear; for optically thick disks with ice (diamonds), $K - H_2O$ is much bluer than that without ice and $H_2O - L'$ is much redder than that without ice, because of the prominent absorption in H_2O band. Note that $K - H_2O$ becomes blue even if a large ($\gtrsim 1 \mu\text{m}$) dust size which makes gray scattering in $K - L'$. Thus, we can conclude that there is H_2O icy dust with a large size if we observe neutral $K - L'$ and blue $K - H_2O$ colors. On the other hand, we can conclude that there is H_2O ice only if we observe red $H_2O - L'$ because the red color is not produced without H_2O ice.

For optically thin disks with ice (squares), $K - H_2O$ starts from the Rayleigh-Jeans color (i.e. much redder color than that without ice) and becomes gradually bluer as grain size becomes larger.

² We used the machine readable form downloaded from the Subaru/CIAO web page; <http://subarutelescope.org/Observing/Instruments/CIAO/camera/sensitivity.html>

³ In this paper, we do not consider any specific size distribution function of the dust particle, but consider a “typical” size of the particle. This “typical” size can be defined by an average over the size distribution function with a certain weight, for example, cross section in a certain band. We can consider a “typical” size of the interstellar dust to be $\sim 0.1 \mu\text{m}$.

$H_2O - L'$ oppositely starts from a very blue color and becomes gradually redder as grain size becomes larger. Such behaviors are caused by the resonance feature in H_2O band seen in the scattering cross section (Fig. 2 [d]).

Interestingly, these differences caused by the feature in H_2O band enable us to classify disk and dust properties on a two color diagram, for example $K - H_2O$ and $K - L'$, as shown in Fig. 5. In this figure, we find four sequences: the optically thick disk with silicate (open circles), the optically thick disk with silicate and ice (filled diamonds), the optically thin disk with silicate (open triangles), and the optically thin disk with silicate and ice (filled squares). Each sequence consists of five points corresponding to the grain sizes of 0.1, 0.3, 1.0, 3.0, and 10 μm . The large asterisk indicates the location expected from the Rayleigh-Jeans law. In Fig. 5, we find five classifications:

- A:** optically thick and thin disks with small ($\lesssim 1 \mu\text{m}$) silicate dust
- B:** optically thick and thin disks with large ($\gtrsim 1 \mu\text{m}$) silicate dust
- C:** optically thick disks with small ($\lesssim 1 \mu\text{m}$) silicate and ice dust
- D:** optically thick and thin disks with large ($\gtrsim 1 \mu\text{m}$) silicate and ice dust
- E:** optically thin disks with small ($\lesssim 1 \mu\text{m}$) silicate and ice dust

If we observe a disk through 3 bands, K , H_2O , and L' , then, we plot the data on the two color diagram, we can judge if the disk is optically thick or thin, the grain size is smaller or larger than about 1 μm , and the dust includes ice or not. Importantly, if we plot spatially resolved data on the diagram, we can derive the dust properties at each position on the disk. That is, we can derive the spatially resolved “snow line” by this method.⁴

Before moving the next section, we briefly comment on the effect of the anisotropic scattering. If the grain size is enough large relative to the wavelength, the scattering becomes a forward scattering not isotropic. In terms of the asymmetry parameter $g \equiv \langle \cos \theta \rangle$ with the scattering angle θ , the NIR photons are scattered with $g > 0.5$ by a 1 μm silicate or H_2O ice grain. In this case, we expect that the disk image in the scattered radiation shows asymmetry; if we observe an inclined disk, the near side becomes brighter by the forward scattering and the other side becomes fainter by an inefficient back scattering. On the other hand, the 3 μm H_2O ice feature may not be affected by the forward scattering because the asymmetry parameter does not show a large variation around the feature.

⁴ The radiation from the hot dust (~ 1000 K) at the disk inner edge is also scattered toward the observer as well as the stellar radiation. This component may make a fraction of the NIR scattered radiation from the disks. This effect could be taken into account by modulating the incident spectrum which has been assumed to be a Planck function (for example in eq. [3]). Note that the modulation of the incident spectrum results in only the change of the reference color. In other words, we could use Figs. 4 and 5 even for such a case if we take a preferable reference color rather than the Rayleigh-Jeans law.

3. Observational feasibility of the “snow line” with current instruments

3.1. Required spatial resolution

H₂O ice condenses on the surface of the dust grains/aggregates if the temperature of the dust surface is low enough (100–200 K depending on the gas density; e.g., Pollack et al. 1994). We estimate the ice existence region in optically thin disks and on the “surface” of optically thick disks. For optically thick disks, only their “surface” is interesting because we cannot observe the scattered stellar radiation from the optically thick interior. When the disk height $z \ll R$, the temperature (T_d) at the “surface” of optically thick disks or in optically thin disks is approximated to

$$\int_0^\infty \kappa_\nu^a B_\nu(T_d[R]) d\nu \approx \frac{1}{4} \left(\frac{R_*}{R} \right)^2 \int_0^\infty \kappa_\nu^a B_\nu(T_*) d\nu, \quad (12)$$

where we have neglected self-absorption of the disk radiation.

The dust temperature calculated from equation (12) is roughly proportional to $R^{-0.5}$ (e.g., Hayashi, Nakazawa, Nakagawa 1985). The absolute value of the temperature depends on the dust composition and size as well as the central stellar luminosity. However, an order of estimate would be enough here. When we assume the stellar effective temperature of 10,000 K and the stellar radius of $2.5 R_\odot$ for an A-type (Herbig Ae/Be) star, and 3,000 K and $2.0 R_\odot$ for a K-type (T Tauri) star, we find that the dust temperature becomes well below of 100 K if $R \gtrsim 100$ AU for the A-type case and $R \gtrsim 10$ AU for the K-type case, implying the presence of “snow line” around that radius.

In order to resolve the disk radius of 10–100 AU at 100 pc away from us, we need to detect the disk scattered light as close as 0.1–1.0 arcsec to the central star. At the same time, we must avoid the central stellar radiation to detect an image of the surrounding very faint scattered light from the disk. Around 3 μm (i.e. H₂O feature), a coronagraphic instrument with an adaptive optics on a 8-m telescope such as CIAO (Coronagraphic Imager with Adaptive Optics) on the 8.2m Subaru Telescope enables us to detect the disk scattered light as close as about 0.75 arcsec (Fukagawa et al. 2006). It is still too large to resolve the expected radius of the “snow line” for the K-type (T Tauri) case ($R \gtrsim 0.1$ arcsec), but is small enough to resolve the “snow line” for the A-type (Herbig) case ($R \gtrsim 1$ arcsec). Thus, we have a chance to detect the “snow line” on the disk around an A-type star with the scattered light.

3.2. Expected brightness

An approximated form of the equation (9) is

$$\frac{I_\nu^{\text{obs}}}{\text{Jy arcsec}^{-2}} \approx 0.076 \left(\frac{T_*}{10^4 \text{ K}} \right) \left(\frac{\lambda}{3.8 \mu\text{m}} \right)^{-2} \left(\frac{R_*}{2.5 R_\odot} \right)^2 \left(\frac{R}{100 \text{ AU}} \right)^{-2} \times \begin{cases} \beta\omega_\nu & (\text{optically thick disk}) \\ \tau_\nu^s & (\text{optically thin disk}) \end{cases}, \quad (13)$$

where we have assumed the Rayleigh-Jeans law, the visible fraction $f_{\text{vis}} = 0.5$, and the H -function $H = 1$. The spectra of the brightness calculated by this equation are shown as the dashed curves in Fig. 3; the good agreements ensure the validity of this approximated equation.

We expect to detect the scattered light even in L' -band ($3.8 \mu\text{m}$) from optically thick (i.e. protoplanetary) disks easily if the observing instrument can resolve the disks at $R \gtrsim 100$ AU with occulting the central star by a coronagraph. For example, we expect that the NIR brightness at 100 AU of an optically thick disk around an A-type star is about $12 \text{ mag arcsec}^{-2}$ for a scattering albedo $\omega \approx 1$ (the dust size of $\gtrsim 1 \mu\text{m}$; see Fig. 2) and a grazing angle $\beta = 0.05$. This is consistent with the observations of Herbig Ae disks ($11\text{--}13 \text{ mag arcsec}^{-2}$; e.g., Augereau et al. 2001; Fukagawa et al. 2004; Fukagawa et al. 2006). Even for the case of a K-type star, the expected brightness at 100 AU is about $14 \text{ mag arcsec}^{-2}$ for $\omega \approx 1$ and $\beta = 0.05$. This is also consistent with the observations of T Tauri disks ($14\text{--}16 \text{ mag arcsec}^{-2}$; e.g., McCabe, Duchêne, Ghez 2002; Weinberger et al. 2002; Schneider et al. 2003).

Such brightness would be easily detected with a coronagraphic instrument on a 8-m telescope. In order to clarify if ice exists on the surface of the disk, we need to achieve H_2O ($3 \mu\text{m}$) $\gtrsim L' + 1$ mag (see Fig. 4 [c]). This would not be difficult because the sensitivity at $3 \mu\text{m}$ is usually better than that at L' -band.

For an optically thin (i.e. debris) disk, we assume the scattering optical depth of $\tau_\nu^s = 10^{-3}$ which is based on the dust mass estimation in debris disks with the SCUBA (Williams, Andrews 2006). In this case, the expected NIR brightness at 100 AU of the disk is about $16 \text{ mag arcsec}^{-2}$ for an A-type star. This is consistent with the observations of debris disks ($15\text{--}16 \text{ mag arcsec}^{-2}$; e.g., Golimowski et al. 2006; Schneider et al. 2006). For a K-type star, the expected brightness is about $18 \text{ mag arcsec}^{-2}$, which is also consistent with that of AU Mic (Metchev et al. 2005). Thus, detecting debris disks in L' band may not be easy with ground-based telescopes even for an A-type star case. With a space instrument, the spatial resolution is the matter rather than the sensitivity.

4. Summary

We have proposed a new method for obtaining the spatially resolved “snow line” in the circumstellar disks; observing $3 \mu\text{m}$ H_2O ice feature in the scattered light. Based on radiative transfer considerations, we show that the frequency dependence of the scattered light comes from the frequency dependence of the albedo for optically thick disks and of the scattering cross section for optically thin disks. Since $3 \mu\text{m}$ H_2O ice feature is clearly imprinted in the albedo and the scattering cross section, we expect to find the feature in the scattered light easily. Then, we have proposed a diagnostics of disk dust properties by near-infrared three bands (K , H_2O , and L') photometry; on the $K - H_2O$ and $K - L'$ two color diagram, we can distinguish that the disk is optically thick or thin, typical grain size is small or large, and ice exists or not. Finally, we have confirmed the scattered light and the H_2O ice feature from protoplanetary disks are detectable and spatially resolvable with a current coronagraphic instrument on 8-m telescopes.

We are grateful to Dr. M. Fukagawa for providing us with informations of the recent brightness measurements of protoplanetary and debris disks. We are also grateful to Drs. M. Ishii, H. Terada,

N. Takato, Y. K. Okamoto and H. Kawakita for useful comments.

References

- Augereau, J. C., Lagrange, A. M., Mouillet, D., & Ménard, F. 2001, *A&A*, 365, 78
- Bertie, J. E., Labbé, H. J., & Whalley, E. 1969, *J. Chem. Phys.*, 50, 4501
- Bohren, C. F., & Huffman, D. R. 1983, *Absorption and Scattering of Light by Small Particles*, Wiley, New York
- Bridgeman, T. 1988, *The Observatory*, 108, 96
- Burrows, C. J., Stapelfeldt, K. R., Watson, A. M., Krist, J. E., Ballester, G. E., Clarke, J. T., Crisp, D., Gallagher, J. S., et al. 1996, *ApJ*, 473, 437
- Chandrasekhar, S. 1960, *Radiative Transfer*, Dover, New York
- Cohen, M., Walker, R. G., Barlow, M. J., & Deacon, J. R. 1992, *AJ*, 104, 1650
- D'Alessio, P., Calvet, N., Hartmann, L., Franco-Hernández, R., Servín, H. 2006, *ApJ*, 638, 314
- Draine, B. T. 1985, *ApJS*, 57, 587
- Dullemond, C. P., van Zadelhoff, G. J., Natta, A. 2002, *A&A*, 389, 464
- Eisner, J. A. 2007, *Nature* 44, 562
- Fukagawa, M., Hayashi, M., Tamura, M., Itoh, Y., Hayashi, S. S., Oasa, Y., Takeuchi, T., Morino, J-I., et al. 2004, *ApJ*, 605, L53
- Fukagawa, M., Tamura, M., Itoh, Y., Kudo, T., Imaeda, Y., Oasa, Y., Hayashi, S. S., & Hayashi, M. 2006, *ApJ*, 636, L153
- Gibb, E. L., Whittet, D. C. B., Boogert, A. C. A., & Tielens, A. G. G. M. 2004, *ApJS*, 151, 35
- Golimowski, D. A., Ardila, D. R., Krist, J. E., Clampin, M., Ford, H. C., Illingworth, G. D., Bartko, F., Benítez, N., et al. 2006, *AJ*, 131, 3109
- Grigorieva, A., Thébault, P., Artymowicz, P., & Brandeker, A. 2007, *A&A*, in press (arXiv:0709.0811v1)
- Hayashi, C., Nakazawa, K., & Nakagawa, Y. 1985, in *Protostars and Planets II*, ed. D. C. Black & M. S. Mathews (Tucson: Univ. Arizona Press) 1100
- Irvine, W. M., & Pollack, J. B. 1968, *Icarus*, 8, 324
- Kalas, P., Fitzgerald, M. P., & Graham, J. R. 2007, *ApJ*, 661, L85
- Kokubo, E., & Ida, S. 2002, *ApJ*, 581, 666
- Koresko, C. D. 1998, *ApJ*, 507, L145
- Krist, J. E., Ardila, D. R., Golimowski, D. A., Clampin, M., Ford, H. C., Illingworth, G. D., Hartig, G. F., Bartko, F., et al. 2005, *AJ*, 129, 1008
- Lin, D. N. C., & Papaloizou, J. 1980, *MNRAS* 191, 37
- Malfait, K., Waelkens, C., Bouwman, J., de Koter, A., & Waters, L. B. F. M. 1999, *A&A*, 345, 181
- McCabe, C., Duchêne, G., Ghez, A. M. 2002, *ApJ*, 575, 974
- McCabe, C., Duchêne, G., Ghez, A. M. 2003, *ApJ*, 588, L113
- Metchev, S. A., Eisner, J. A., Hillenbrand, L. A., & Wolf, S. 2005, *ApJ*, 622, 451
- Miyake, K., & Nakagawa, Y. 1993, *Icarus*, 106, 20
- Morbidelli, A., Chambers, J., Lunine, J. I., Petit, J. M., Robert, F., Valsecchi, G. B., & Cyr, K. E. 2000, *Meteoritics and Planetary Science*, 35, 1309
- Oka, A., Ikoma, M., Ida, S., & Nakamoto, T. 2008, in preparation

Preibisch, Th., Ossenkopf, V., York, H. W., Henning, Th. 1993, A&A, 279, 577
Pollack, J. B., et al. 1994, ApJ, 421, 615
Raymond, S. N., Quinn, T., & Lunine, J. I. 2004, Icarus 168, 1
Schaaf, J. W., & Williams, D. 1973, J. Opt. Soc. America, 63, 726
Schneider, G., Wood, K., Silverstone, M. D., Hines, D. C., Koerner, D. W., Whitney, B. A., Bjorkman, J. E., & Lowrance, P. J. 2003, AJ, 125, 1467
Schneider, G., Silverstone, M. D., Hines, D. C., Augereau, J.-., Pinte, C., Ménard, F., Krist, J., Clampin, M., et al. 2006, ApJ, 650, 414
Smith, B. A., & Terile, R. J. 1984, Science, 226, 1421
Terada, H., Tokunaga, A. T., Kobayashi, N., Takato, N., Hayano, Y., Takami, H. 2007, ApJ, 667, 303
Weinberger, A. J., Becklin, E. E., Schneider, G., Chiang, E. I., Lowrance, P. J., Silverstone, M., Zuckerman, B., Hines, D. C., & Smith, B. A. 2002, ApJ, 566, 409
Williams, J. P., & Andrews, S. M. 2006, ApJ, 653, 1480
Yurimoto, H., & Kuramoto, K. 2002, Science, 305, 1763

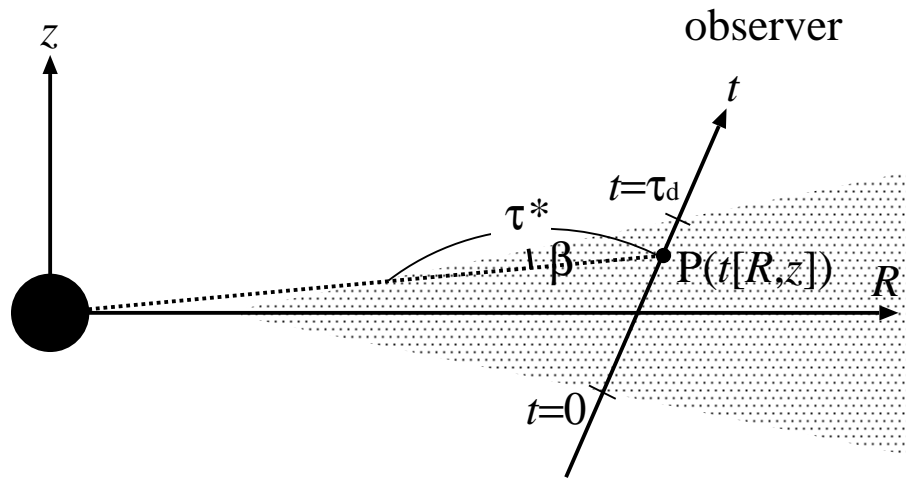


Fig. 1. Schematic figure of the considered geometry.

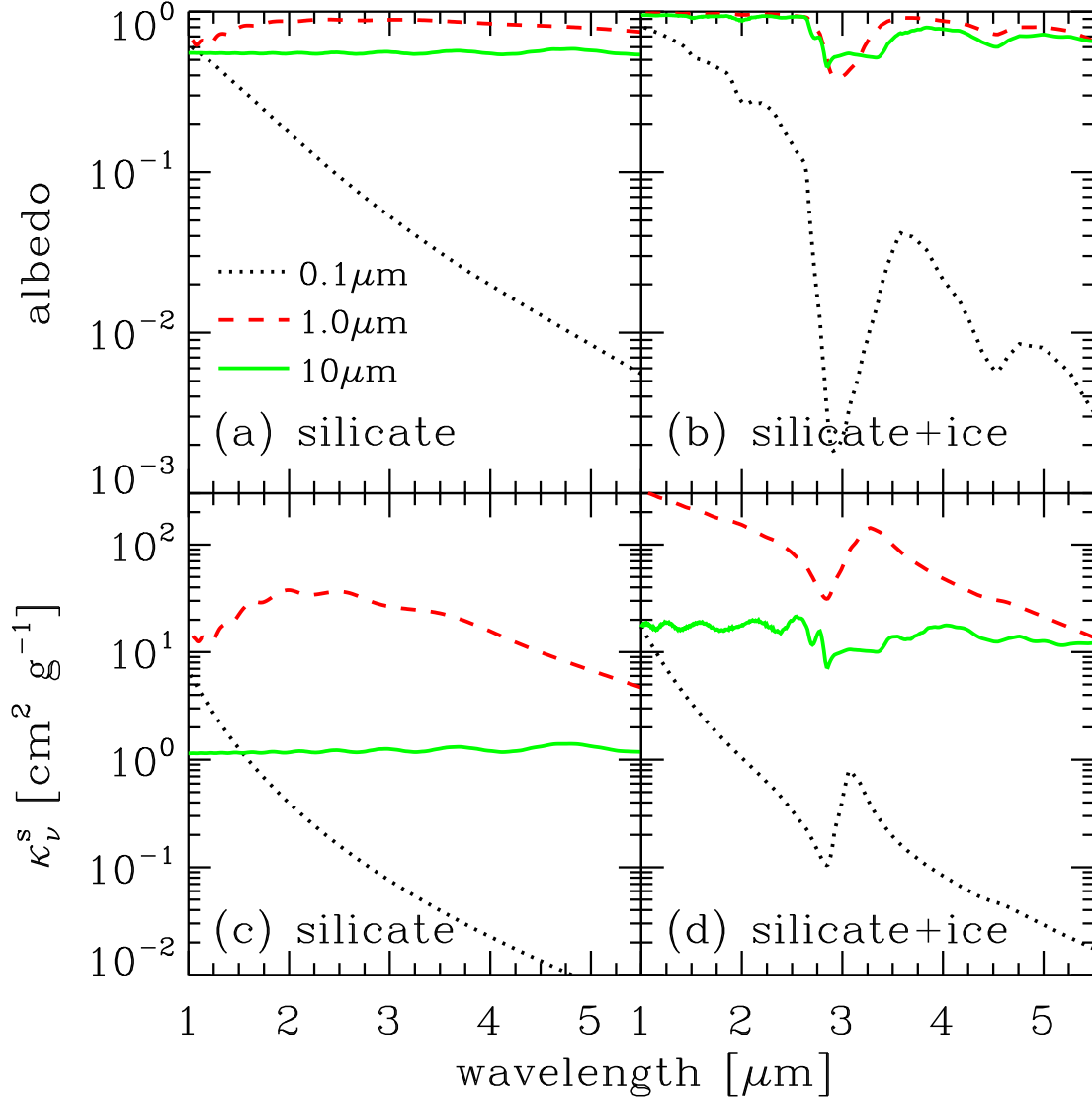


Fig. 2. Scattering albedos and cross sections: (a) albedo of silicate dust, (b) albedo of silicate and H_2O ice dust, (c) cross section per unit gas mass of silicate dust, and (d) cross section per unit gas mass of silicate and H_2O ice dust. The assumed mass abundances of silicate and H_2O ice relative to gas are 0.0043 and 0.0094, respectively (Miyake & Nakagawa 1993). The solid, dashed, and dotted lines are the cases with the grain size of 10, 1, and $0.1 \mu\text{m}$, respectively.

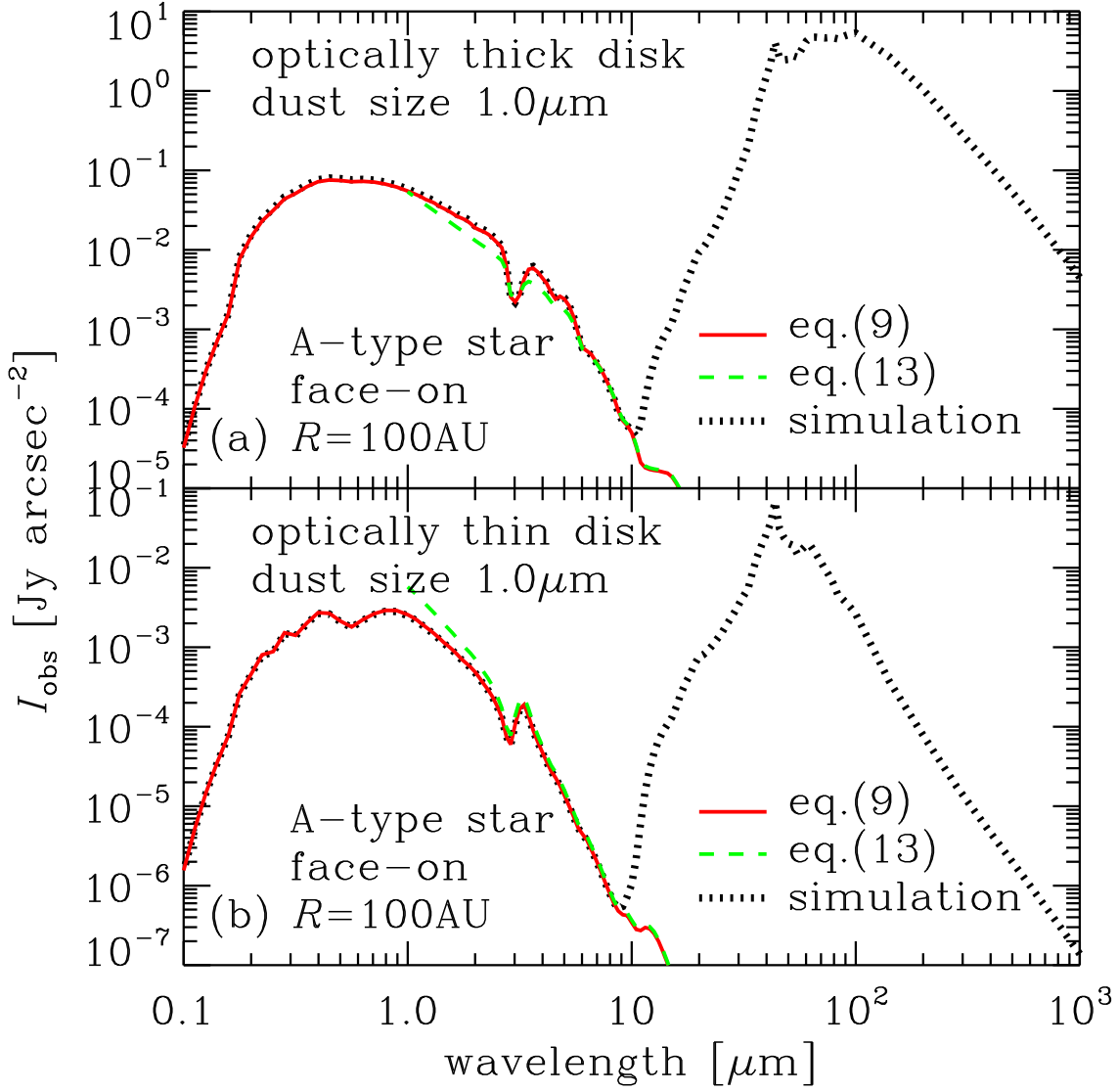


Fig. 3. Expected spectra of the face-on brightness of an annulus with the radius 100 AU around a central A-type star: (a) optically thick case and (b) optically thin case. The assumed dust is $1.0\mu\text{m}$ silicate and H_2O ice. The solid curves are analytic models of the scattered light expressed in eq. (9), the dashed curves are simpler models of the scattered light expressed in eq. (13), and the dotted curves are the scattered and the thermal radiations of the annulus from numerical radiative transfer simulations.

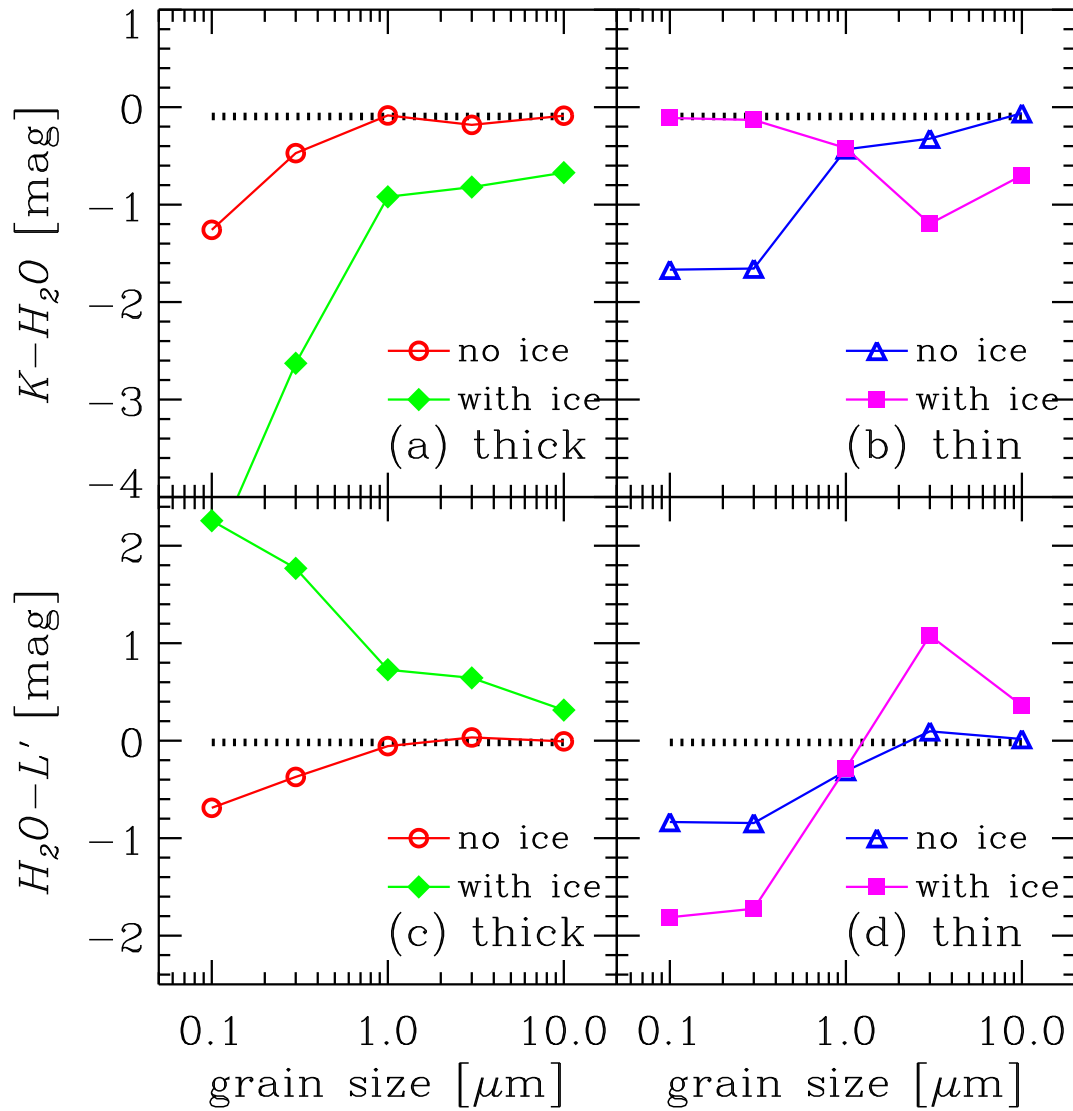


Fig. 4. Expected colors of the scattered light as a function of the dust size: (a) $K - H_2O$ for optically thick case, (b) $K - H_2O$ for optically thin case, (c) $H_2O - L'$ for optically thick case, and (d) $H_2O - L'$ for optically thin case. In each panel, open symbols are silicate dust and filled symbols are silicate and ice dust. The dotted line is the Rayleigh-Jeans law. The unit of the vertical axis is the Vega magnitude.

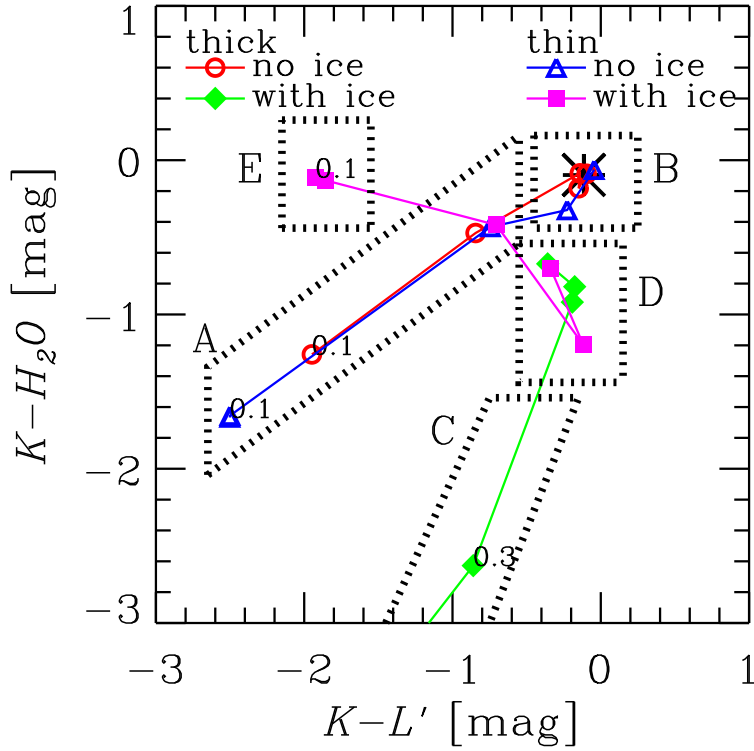


Fig. 5. Expected two color diagram. The circles, diamonds, triangles, and squares are the cases of the optically thick disk with silicate, the optically thick disk with silicate and ice, the optically thin disk with silicate, and the optically thin disk with silicate and ice, respectively. Each sequence with the same symbol is the sequence of the grain size: 0.1, 0.3, 1, 3, and 10 μm . The labels on some points indicate the dust size in μm . The triangles for 0.1 and 0.3 μm are almost overlaid. The large asterisk is the location of the Rayleigh-Jeans law. The areas surrounded by dotted lines show the five classifications on the diagram (see the text). The units of the axes are the Vega magnitude.